PHYSICAL REVIEW D **92,** 056005 (2015)

High energy density in multisoliton collisions

Danial Saadatmand,[1,2,*] Sergey V. Dmitriev,[3,4,†] and Panayotis G. Kevrekidis[5,‡]
[1]*Department of Physics, Ferdowsi University of Mashhad, 91775-1436 Mashhad, Iran*
[2]*Department of Physics, University of Sistan and Baluchestan, Zahedan, Iran*
[3]*Institute for Metals Superplasticity Problems RAS, Khalturin Street 39, 450001 Ufa, Russia*
[4]*Research Laboratory for Mechanics of New Nanomaterials,*
Peter the Great St. Petersburg Polytechnical University, St. Petersburg 195251, Russia
[5]*Department of Mathematics and Statistics, University of Massachusetts,*
Amherst, Massachusetts 01003, USA
(Received 1 June 2015; published 21 September 2015)

Solitons are very effective in transporting energy over great distances and collisions between them can produce high energy density spots of relevance to phase transformations, energy localization and defect formation among others. It is then important to study how energy density accumulation scales in multisoliton collisions. In this study, we demonstrate that the maximal energy density that can be achieved in collision of N slowly moving kinks and antikinks in the integrable sine-Gordon field, remarkably, is proportional to N^2, while the total energy of the system is proportional to N. This maximal energy density can be achieved only if the difference between the number of colliding kinks and antikinks is minimal, i.e., is equal to 0 for even N and 1 for odd N and if the pattern involves an alternating array of kinks and antikinks. Interestingly, for odd (even) N the maximal energy density appears in the form of potential (kinetic) energy, while kinetic (potential) energy is equal to zero. The results of the present study rely on the analysis of the exact multisoliton solutions for $N = 1, 2$, and 3 and on the numerical simulation results for $N = 4, 5, 6$, and 7. The effect of weak Hamiltonian and non-Hamiltonian perturbations on the maximal energy density in multikink collisions is also discussed as well as that of the collision relative phase. Based on these results one can speculate that the soliton collisions in the sine-Gordon field can, in principle, controllably produce very high energy density. This can have important consequences for many physical phenomena described by the Klein-Gordon equations.

DOI: 10.1103/PhysRevD.92.056005 PACS numbers: 05.45.Yv, 11.10.Lm, 45.50.Tn

I. INTRODUCTION

The celebrated sine-Gordon equation (SGE) [1,2],

$$\phi_{tt} - \phi_{xx} + \sin\phi = 0, \tag{1}$$

has emerged in the geometry of surfaces [3] and then it has long been used in physics to describe propagation of magnetic flux on an array of superconducting Josephson junctions [4], to study the interacting mesons and baryons [5], fermions in the Thirring model [6], the properties of crystal dislocations [7], dynamics of domain walls in ferromagnetics [8] and ferroelectrics [9,10], the oscillations of an array of pendula [11], and others [2,7,12,13].

The SGE is capable of describing the dynamics of topological solitons such as a kink and an antikink, as well as their bound state called breather, a feature that distinguishes it from other continuum models [14]. Multisoliton solutions to Eq. (1) have been derived with the help of the Bäcklund transformation [15,16] or the Hirota method [17,18].

However, in addition to its importance in classical mechanics and also e.g. in condensed matter physics (see e.g. [19] for a relatively recent example of its use for the description of the Beresinskii-Kosterlitz-Thouless vortices in superconductors), it is also an important model in high energy physics. In the latter context, in addition to its connection to supersymmetric field theories [20] and string theory [21], it has also been argued to be related to exotic structures at the interface of fields and effective particles, such as oscillons [22] and Skyrmions (when trapped by vortices) [23], among others. Hence, it remains a topic of extensive interest not only within nonlinear waves but also principally within the theme of fields and elementary particles.

In the present work, we focus on the energy density arising from the interaction of prototypical nonlinear structures within the SGE model. The energy density has a maximum in the kink's core and vanishes away from it. A moving kink transports this energy as its center of mass moves and hence kink collisions can result in an increase of the energy density. For applications it is important to know what is the largest energy density that can be accumulated in multikink collisions. Such manifestations of large energy density can be associated with

*saadatmand.d@gmail.com
†dmitriev.sergey.v@gmail.com
‡kevrekid@math.umass.edu

rogue events (i.e., the formation of rogue waves; see e.g. the reviews of [24,25]), which have been of extreme interest in recent years. More generally, they can be used for targeted energy localization which is of interest in its own right.

In this paper, we calculate the maximal energy density that can be achieved in the collision of N slowly moving sine-Gordon kinks and antikinks for $N \leq 7$. The question is, can the cores of all N colliding solitons merge at one point, and if yes, what is the maximal energy density at the collision point? The answers can be readily found in the concluding Sec. V and the way they were obtained is described in Sec. III, which follows Sec. II with preliminary remarks and a description of the simulation method. In Sec. IV we discuss the effect of perturbations and the effect of inaccuracy in the initial conditions on the maximal energy density in multisoliton collisions. The key result of our considerations is the unexpected scaling of the maximal energy density (proportional to N^2) with the number of solitons N. Furthermore, conditions (on the structure of the soliton pattern) and manifestations of the energy localization are illustrated in the process.

II. PRELIMINARY REMARKS

During the dynamics of Eq. (1) the total energy is conserved as

$$E = K + P, \tag{2}$$

which is the sum of the kinetic and potential energies given, respectively, by

$$K = \int_{-\infty}^{\infty} \frac{1}{2}\phi_t^2 dx, \qquad P = \int_{-\infty}^{\infty} \left(\frac{1}{2}\phi_x^2 + 1 - \cos\phi\right) dx. \tag{3}$$

The kinetic energy density and the potential energy density of the SGE field are given by the integrands of Eq. (3),

$$k(x,t) = \frac{1}{2}\phi_t^2, \qquad p(x,t) = \frac{1}{2}\phi_x^2 + 1 - \cos\phi, \tag{4}$$

and the total energy density is

$$e(x,t) = k(x,t) + p(x,t). \tag{5}$$

The two basic soliton solutions to SGE (1) are the kink (antikink)

$$\phi(x,t) = \pm 4 \arctan\{\exp[\delta_k(x - V_k t)]\}, \tag{6}$$

and the breather

$$\phi(x,t) = 4 \arctan \frac{\eta \sin[\delta_b \omega (t - V_b x)]}{\omega \cosh[\delta_b \eta (x - V_b t)]}, \tag{7}$$

where V_k is kink velocity; V_b, ω are the breather velocity and frequency; and

$$\delta_{k,b} = \frac{1}{\sqrt{1 - V_{k,b}^2}}, \qquad \eta = \sqrt{1 - \omega^2}. \tag{8}$$

The upper (lower) sign in Eq. (6) corresponds to the kink (antikink). The breather solution Eq. (7) can be regarded as a kink-antikink bound state [26–28].

A collision between two kinks having velocities $\pm V_k$ is described by the following solution to Eq. (1):

$$\phi(x,t) = 4 \arctan \frac{V_k \sinh(\delta_k x)}{\cosh(\delta_k V_k t)}. \tag{9}$$

For the collision between kink and antikink having velocities $\pm V_k$ one has the exact solution

$$\phi(x,t) = 4 \arctan \frac{V_k \cosh(\delta_k x)}{\sinh(\delta_k V_k t)}. \tag{10}$$

Substituting Eq. (6) and Eq. (7) into Eq. (2) one finds the total energies of the kink and breather

$$E_k = 8\delta_k, \qquad E_b = 16\delta_k \eta. \tag{11}$$

We are not interested in the relativistic effects and only slow solitons ($V_k \ll 1$, $V_b \ll 1$) will be considered so that $\delta_k \approx 1$ and $\delta_b \approx 1$. Only low-frequency breathers ($\omega \ll 1$) will be discussed so that $\eta \approx 1$. Then, we can write approximately that $E_k \approx 8$ and $E_b \approx 16$.

Even though the analytical expressions for multisoliton solutions to SGE are available [15–17] their complexity increases rapidly with the number of solitons, N. That is why for $N \geq 4$ we will do calculations numerically. For this we discretize Eq. (1) as follows:

$$\begin{aligned} &\frac{d^2\phi_n}{dt^2} - \frac{1}{h^2}(\phi_{n-1} - 2\phi_n + \phi_{n+1}) \\ &\quad + \frac{1}{12h^2}(\phi_{n-2} - 4\phi_{n-1} + 6\phi_n - 4\phi_{n+1} + \phi_{n+2}) \\ &\quad + \sin\phi_n = 0, \end{aligned} \tag{12}$$

where h is the lattice spacing; $n = 0, \pm 1, \pm 2, \ldots$; and $\phi_n(t) = \phi(nh, t)$. To minimize the effect of discreteness, the term ϕ_{xx} in Eq. (1) is discretized with the accuracy $O(h^4)$, which has been used previously [7,13,29]. The equations of motion in the form of Eq. (12) were integrated with respect to the time using an explicit scheme with the time step τ and the accuracy of $O(\tau^4)$. The simulations reported in Sec. III were carried out for $h = 0.1$, $h = 0.05$ and $\tau = 0.005$.

Before we start the presentation of the main results the following remark should be made. Two kinks (or two

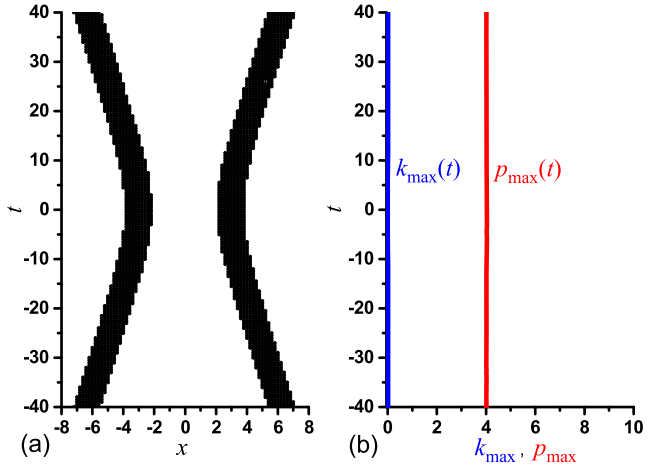

FIG. 1 (color online). Collision of two kinks having velocities $V_k = \pm 0.1$ according to Eq. (9). (a) Trajectories of the soliton cores are shown by the regions where total energy density $e(x,t) > 2$. (b) Maximal over spatial coordinate kinetic (blue) and potential (red) energy densities as the functions of time. Maximal energy density does not grow during collision of solitons having the same topological charge because they repel each other and their cores do not merge.

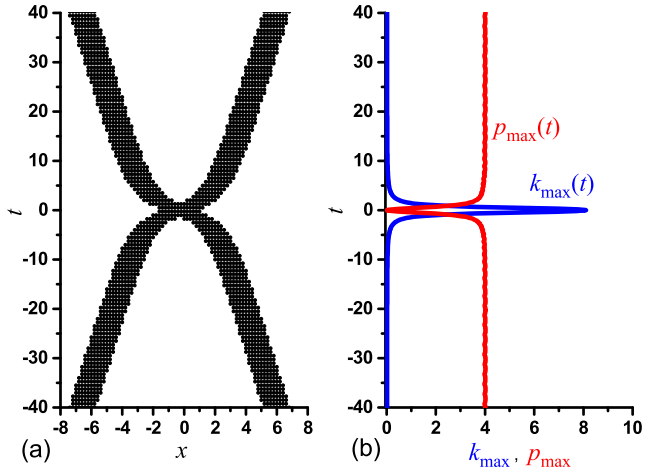

FIG. 2 (color online). Same as in Fig. 1 but for the collision of a kink and an antikink given by Eq. (10) with subkink velocities $V_k = \pm 0.1$. Cores of the mutually attractive solitons merge at the collision point and total energy density at the collision point $e(x,0) = k(x,0) + p(x,0)$ rises up to about 8.

antikinks) repel each other as quasiparticles having the same topological charge. When they collide, they bounce off each other, their cores do not merge and, consequently, the maximal energy density does not grow. This is illustrated by Fig. 1, where for the solution Eq. (9) with $V_k = 0.1$ we show (a) the regions of the (x,t) plane where the total energy density $e(x,t) > 2$ and (b) the maximal over x densities of kinetic (blue line) and potential (red line) energies. The kinks collide at $t = 0, x = 0$. One can see that $k_{max}(t)$ is nearly zero (due to the small kink velocity and the quadratic dependence on it), while $p_{max}(t) \approx 4$, and these values are not affected by the collision.

On the contrary, kink and antikink are mutually attractive quasiparticles. Their cores merge during collision and the maximal energy density increases at the collision point. This can be seen in Fig. 2 where the kink-antikink solution Eq. (10) is presented for $V_k = 0.1$. Far from the collision $(t = 0,\ x = 0)$ we have $k_{max}(t) \approx 0$ and $p_{max}(t) \approx 4$. However, at $t = 0$ p_{max} drops to zero, while k_{max} rises up to nearly 8, and so does the maximal total energy density e_{max} (not shown in the figure).

In Fig. 3 similar results are shown for the breather solution Eq. (7) with $V_b = 0$ and $\omega = 0.1$. It was already mentioned that the low-frequency breather can be envisioned as a kink-antikink bound state, and when the subkinks collide, p_{max} drops to zero and k_{max} reaches the value of nearly 8, as does e_{max}. In the breather case, instead of this happening once (as in Fig. 2) the phenomenology periodically repeats itself, due to the time periodicity of the state.

For the three-kink solutions it has been demonstrated that the cores of all three kinks can merge only if they collide in the spatial arrangement kink-antikink-kink (or antikink-kink-antikink) [30]. This is understandable because in the combinations such as kink-kink-kink or kink-kink-antikink the solitons having the same topological charge repel each other because between them there is no soliton of the opposite charge. In the following we will consider the multisoliton solutions with alternating kinks and antikinks. In this case each kink (or antikink) attracts the nearest neighbors of the opposite charge and all of them can collide at one point, as it will be demonstrated in the following section. These types of configurations promote the energy exchange, contrary to what is the case for configurations bearing adjacent waves of the same type.

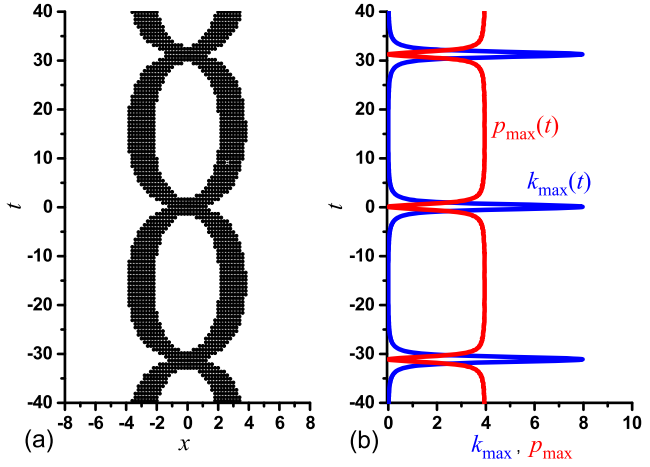

FIG. 3 (color online). Same as in Fig. 1 but for the breather given by Eq. (7) with $V_b = 0$ and $\omega = 0.1$. When the subkinks collide, the potential energy density is almost zero and the kinetic energy density is about 8.

III. MAXIMAL ENERGY DENSITY OF MULTISOLITON SOLUTIONS TO THE SGE

A. Case $N = 1$

For a standing kink, Eq. (6) with $V_k = 0$, the kinetic energy is zero. Then, the total energy density can be found from Eqs. (4)–(5) in the form

$$e(x) = p(x) = 8\left(\frac{e^x}{1+e^{2x}}\right)^2 + 1 - \cos(4\arctan e^x). \quad (13)$$

This function has a maximum at $x = 0$, which is the coordinate of the kink's center. The value of the maximal energy density of the standing kink is

$$e^{(1)}_{\max} = p^{(1)}_{\max} = 4. \quad (14)$$

B. Case $N = 2$

The breather solution (7) for $V_b = 0$ in the limit $\omega \to 0$, and the kink-antikink solution (10) in the limit $V_k \to 0$ both approach the same separatrix two-soliton solution

$$\phi(x,t) = 4\arctan\frac{t}{\cosh x}. \quad (15)$$

This solution describes the kink and antikink that after the collision at $t = 0$ move apart and their velocities vanish as $t \to \infty$. The solution is depicted in Fig. 4 where, as before, in (a) the points of the (x,t) plane with $e(x,t) > 2$ are shown and in (b) the maximal—over the spatial coordinate x—values of kinetic (blue) and potential (red) energy densities are presented as functions of time. We now calculate the exact value of the maximal energy density by substituting Eq. (15) into Eqs. (4)–(5). The calculation can be simplified by noting that at $t = 0$ one has $\phi(x,0) \equiv 0$ and thus, at the collision point the energy of the kink-antikink pair is in the form of kinetic energy,

$$e(x,0) = k(x,0) = \frac{8}{\cosh^2 x}. \quad (16)$$

The energy density has a maximum at the collision point $x = 0$:

$$e^{(2)}_{\max} = k^{(2)}_{\max} = 8. \quad (17)$$

C. Case $N = 3$

The kink-breather (three-soliton) solution to SGE reads

$$\begin{aligned}\phi(x,t) &= 4\arctan(\exp B) + 4\arctan\frac{\eta Y}{\omega Z},\\ Y &= 2\omega(\sinh D - \cos C \sinh B)\\ &\quad + 2\delta_b\delta_k(V_k - V_b)\sin C\cosh B,\\ Z &= 2\eta(\cos C + \sinh D \sinh B)\\ &\quad - 2\delta_b\delta_k(1 - V_kV_b)\cosh D\cosh B,\\ B &= \delta_k(x - V_kt),\\ C &= -\omega\delta_b(t - V_bx), \qquad D = \eta\delta_b(x - V_bt). \end{aligned} \quad (18)$$

In the limit $V_k \to 0$, $V_b \to 0$, and $\omega \to 0$, this solution assumes the following form [see Eq. (26) of Ref. [31]]:

$$\phi(x,t) = 4\arctan e^x + 4\arctan\frac{x\cosh x - t^2\sinh x}{t^2 + \cosh^2 x}. \quad (19)$$

This separatrix solution describes the antikink standing at $x = 0$ and two kinks that after the collision with the antikink at $t = 0$ move apart and their velocities vanish as $t \to 0$. The solution is presented in Fig. 5 using a visualization similar to the previous figures.

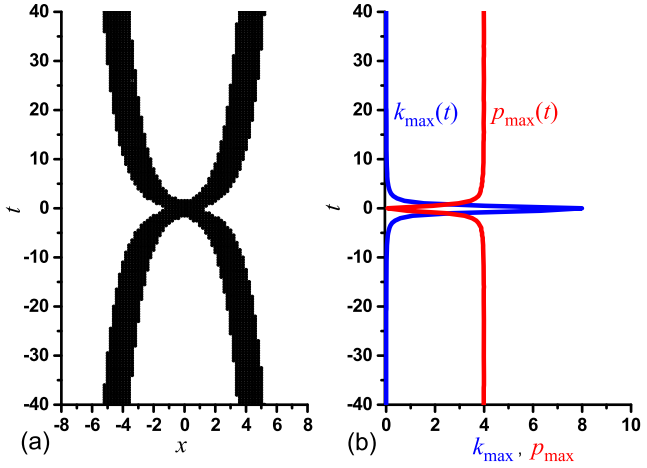

FIG. 4 (color online). Same as in Fig. 1 but for the separatrix two-soliton solution of Eq. (15). When the kink and antikink collide the potential energy density is equal to zero and kinetic energy density is exactly 8.

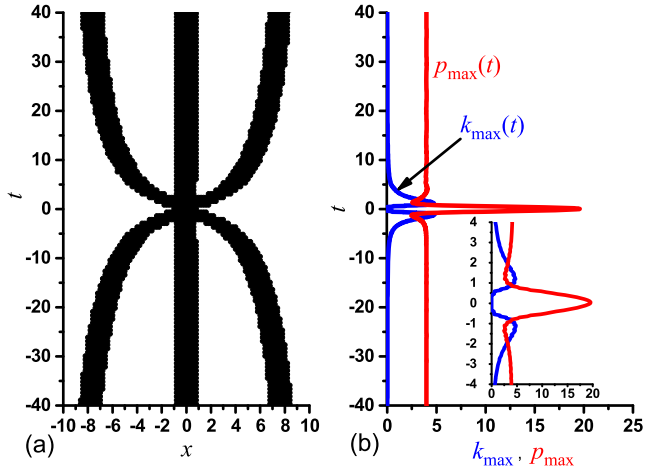

FIG. 5 (color online). Same as in Fig. 1 but for the separatrix three-soliton solution Eq. (19). The inset shows the blowup of the region around $t = 0$. When the two kinks collide with the antikink, the kinetic energy density is equal to zero and the potential energy density is exactly 20.

To calculate the exact value of the maximal energy density, we again substitute Eq. (19) into Eqs. (4)–(5). Note that at $t = 0$ one has $\phi_t(x, 0) \equiv 0$ and thus, at the collision point the energy of the kink-antikink-kink solution is in the form of potential energy,

$$e(x,0) = p(x,0) = 8\left(\frac{e^x}{1+e^{2x}} + \frac{\cosh x - x\sinh x}{\cosh^2 x + x^2}\right)^2 + 1 - \cos\left(4\arctan e^x + 4\arctan\frac{x}{\cosh x}\right). \quad (20)$$

The energy density has a maximum at the collision point $x = 0$:

$$e^{(3)}_{\max} = p^{(3)}_{\max} = 20. \quad (21)$$

D. Case $N = 4$

The solution to SGE that describes collision of two breathers (i.e., a four-soliton solution) with velocities V_1, V_2 and frequencies ω_1, ω_2 is given by

$$\begin{aligned}
\phi(x,t) &= 4\arctan(S) - 4\arctan\frac{\eta_2(T\cosh B_1 + \sin C_1)}{\omega_2(\cosh B_1 + T\sin C_1)},\\
T &= \varphi\frac{2\tau[(S-P)(1+SP) - Q^2S] - 2\beta Q(1+S^2)}{\varphi^2[(1+S)(1+SP) + Q^2S^2] + (\tau^2+\beta^2)[(S-P)^2+Q^2]},\\
P &= \frac{\beta X + \kappa Y}{\varepsilon Z}, \qquad Q = \frac{\beta Y - \kappa X}{\varepsilon Z}, \qquad S = \frac{\eta_1\sin C_1}{\cosh B_1\omega_1},\\
X &= \sinh B_2\cos C_1 - \cos C_2\sinh B_1, \qquad Y = \cosh B_2\sin C_1 + \sin C_2\cosh B_1,\\
Z &= \cos(C_1 - C_2) + \cosh(B_1 + B_2),\\
B_{1,2} &= \eta_{1,2}\delta_{1,2}(x - x_{1,2} - V_{1,2}t), \qquad C_{1,2} = \Delta_{1,2} - \omega_{1,2}\delta_{1,2}[t - (x - x_{1,2})V_{1,2}],\\
\delta_{1,2} &= (1 - V^2_{1,2})^{-1/2}, \qquad \eta_{1,2} = (1 - \omega^2_{1,2})^{1/2}, \qquad \alpha = \frac{\delta_2(1+V_2)}{\delta_1(1+V_1)},\\
\beta &= \alpha - 1/\alpha, \qquad \varepsilon = 2\alpha - \beta + 2(\omega_1\omega_2 - \eta_1\eta_2), \qquad \tau = 2(\omega_1\eta_2 - \eta_1\omega_2),\\
\varphi &= 2\alpha - \beta - 2(\omega_1\omega_2 + \eta_1\eta_2), \qquad \kappa = 2(\omega_1\eta_2 + \eta_1\omega_2).
\end{aligned} \quad (22)$$

Here $x_{1,2}$ and $\Delta_{1,2}$ define initial positions and initial phases of the two breathers, respectively.

It is possible to derive the separatrix solution from Eq. (22) in the limits $V_{1,2} \to 0$ and $\omega_{1,2} \to 0$ but the derivation is tedious and for $N > 3$ we calculate the maximal energy density numerically considering collisions of slow kinks or slow, low-frequency breathers. Parameters of the colliding solitons are chosen to achieve collision of all N subkinks at one point. Note that the collisions of two slow, low-frequency breathers were analyzed earlier in the study of fractal soliton collisions and the possibility for all four subkinks to collide at one point was demonstrated in Ref. [32].

Equations (12) are integrated numerically for $h = 0.1$, $h = 0.05$ and $\tau = 0.005$. Initial conditions are set with the help of Eq. (22). For simplicity, the collision of symmetric slow and low-frequency breathers is considered by setting $V_1 = -V_2 = 0.1$, $\omega_{1,2} = 0.1$, $\Delta_1 = 0$ and $\Delta_2 = \pi$. Note that the out-of-phase (in-phase) breathers collide such that they attract (repel) each other. To achieve the collision of all four subkinks at one point one should choose a proper initial distance between the breathers. In a series of numerical runs it is found that $x_2 - x_1 = 4.012$ gives the desired result presented in Fig. 6.

It can be seen in Fig. 6 that at the point of collision of the four subkinks the potential energy density is almost zero while the kinetic energy density shows a peak with a height nearly equal to 32. More precisely, for $h = 0.1$ the largest energy density we could obtain by varying the parameter $x_2 - x_1$ was 32.21, while for $h = 0.05$ it was 32.05. With decreasing h the accuracy of simulation increases. We thus conclude that the total energy density at the collision point is

$$e^{(4)}_{\max} = k^{(4)}_{\max} \approx 32. \quad (23)$$

Note that after the collision breathers have frequencies and velocities different from the initial values. This is due to the (weak but still nontrivial in this collision phenomenon) effect of discreteness, which breaks the integrability of the model. For more details on the inelasticity of near-separatrix multisoliton collisions in weakly perturbed SGE see Refs. [30–32].

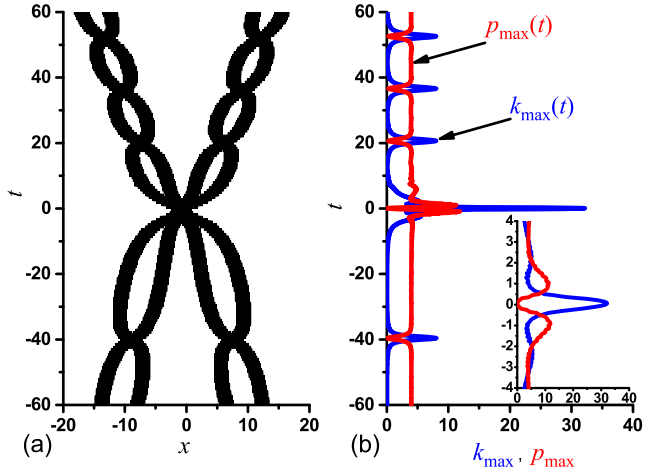

FIG. 6 (color online). The result of the numerical simulation of the collision of two breathers (four subkinks). Initial conditions are set with the help of Eq. (22) with $V_1 = -V_2 = 0.1$, $\omega_{1,2} = 0.1$, $\Delta_1 = 0$ and $\Delta_2 = \pi$, and $x_2 - x_1 = 4.012$. (a) The soliton cores shown by the regions where $e(x,t) > 2$. (b) Maximal—over the spatial coordinate x—kinetic (blue) and potential (red) energy densities as functions of time. The inset shows the curves near $t = 0$. At the collision point, potential energy density is practically zero, while the kinetic energy density increases up to nearly 32.

Practically, it is important to see how sensitive the maximal energy density is to the relative phase of the breathers, $\Delta_2 - \Delta_1$. The result of this numerical study is given in Fig. 7. It can be seen from Fig. 7(a) that to keep the maximal energy density within 10% of the maximal value

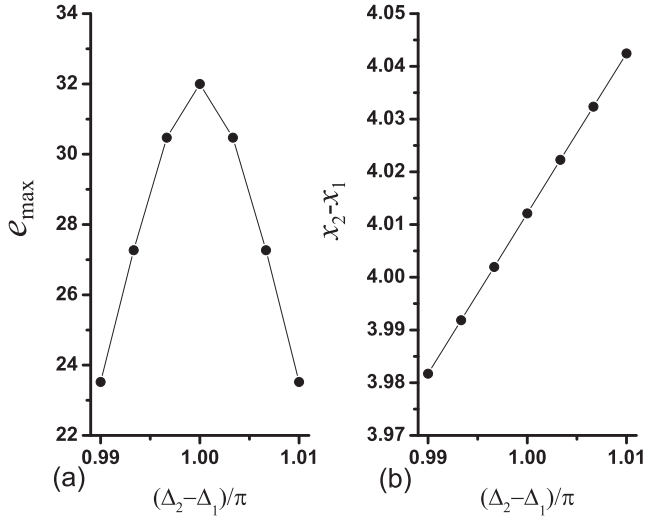

FIG. 7. (a) Maximal energy density in breather-breather collisions as the function of the relative phase of the breathers $(\Delta_2 - \Delta_1)/\pi$. (b) Initial distance between breathers to achieve maximal energy density as a function of $(\Delta_2 - \Delta_1)/\pi$. The breathers have frequencies $\omega_{1,2} = 0.1$ and velocities $V_1 = -V_2 = 0.1$.

observed for $\Delta_2 - \Delta_1 = \pi$, one has to control the phase difference with the accuracy of 0.01π. The initial distance between breathers that leads to the maximal energy density depends on the phase difference as shown in Fig. 7(b). It is clear that the maximal energy density that can be attained in the breather-breather collisions depends not only on their relative phase but also on the initial distance between them. Since the sine-Gordon kinks do not possess an internal phase, it is easier to achieve high energy density spots by colliding kinks and antikinks and controlling their initial positions only. This setting is used in Sec. IV C to further investigate the sensitivity of the maximal energy density in multikink collisions to the initial conditions.

E. Case $N = 5$

Here we set initial conditions using the individual kink (antikink) solution of Eq. (6) [rather than an extremely cumbersome five-soliton solution]. As shown in Fig. 8(a), the initial positions and velocities of the five solitons are chosen such that initially they do not overlap and so that they collide at one point. As it was already mentioned, each soliton should attract its nearest neighbors and thus, it should have the topological charge opposite to that of its neighbors. In our case solitons 1, 3, and 5 are kinks and 2 and 4 are antikinks. The kink 3 is located at the origin and it is at rest, $x_3 = 0$ and $V_3 = 0$. The antikinks 2 and 4 have velocities $V_2 = -V_4 = 0.025$ and initial positions $x_2 = -x_4 = -12.0$. By symmetry the solitons 2, 3, and 4

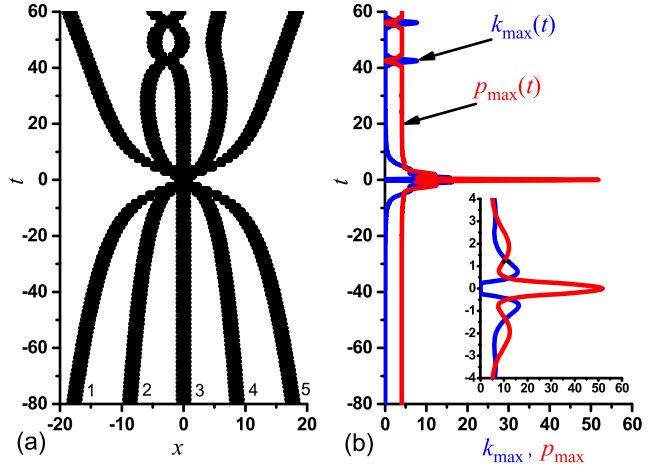

FIG. 8 (color online). Collision of five kinks/antikinks at one point. The choice of initial conditions is described in the text. As before, in (a) the regions of the (x,t) plane with energy density $e(x,t) > 2$ are shown. In (b) the maximal, over x, kinetic and potential energy densities are shown as functions of time by the blue and red lines, respectively. At the collision point the potential energy density features the maximum of about approximately 52, while the kinetic energy density is almost zero. The inset shows the details of the curves near $t = 0$. Note that the solitons are numbered in (a) before the collision. Odd quasiparticles are kinks and even ones are antikinks.

collide at one point. For the kinks 1 and 5 we take two times larger velocities $V_1 = -V_5 = 0.05$ and choose their initial coordinates to achieve the collision of five solitons at one point. This happens for $x_1 = -x_5 = -24.376549$. Although the exactly coincident collision does not happen for exactly double initial distances (from the origin) for double initial velocities, the latter is a reasonable rule of thumb for preparing the initial conditions of the multisoliton configuration; a slight subsequent refinement may then be needed (such as the slight displacement of the outer kinks from $x_1 = -x_5 = 24$ to $x_1 = -x_5 = -24.376549$).

As it can be seen from Fig. 8(b), when the five solitons collide, the maximal kinetic energy density is close to zero, while the maximal potential energy density is 50.93 for $h = 0.1$ and 51.85 for $h = 0.05$. We conclude that

$$e^{(5)}_{\max} = p^{(5)}_{\max} \approx 52. \tag{24}$$

A relevant additional remark here is that the significant role of weak asymmetries (in the preparation of our initial condition) can be observed to be exacerbated in the outcome of the collisional dynamics of Fig. 8. In particular, the figure showcases a visibly asymmetric result of the dynamics featuring, in addition to two outer nearly symmetric kinks, a breather (involving the antikink of soliton 2 and the kink of soliton 3) and a "stray" kink (the antikink of soliton 4). Once again here, the nonintegrability of the underlying numerical scheme is deemed to be responsible for the observed asymmetry, although the energy density accumulation at $x = t = 0$ is expected to persist even for an integrable discretization.

F. Case $N = 6$

Referring to Fig. 9(a), note that the solitons 1, 3, and 5 are kinks and 2, 4, and 6 are antikinks. Initial soliton positions and velocities to achieve their collision at one point are $x_1 = -x_6 = -34.90395$, $V_1 = -V_6 = 0.1$, $x_2 = -x_5 = 19.37864$, $V_2 = -V_5 = 0.05$, $x_3 = -x_4 = -7$, $V_3 = -V_4 = 0.025$. Once again, the velocities have been selected using factors of 2, while the positions have been refined (from the corresponding factors of 2) to ensure that the collision occurs for all solitons at the same point.

From Fig. 9(b) it is clear that at the collision point the maximal, over x, potential energy density is nearly zero while the maximal kinetic energy density reaches its highest attainable value. The height of the maximum is 72.62 for $h = 0.1$ and 72.08 for $h = 0.05$. Thus,

$$e^{(6)}_{\max} = k^{(6)}_{\max} \approx 72. \tag{25}$$

Here, solitons 2 and 3, as well as 4 and 5, merge in the symmetric aftermath of the collision into breather states (a feature that once again would be avoided in the realm of fully integrable dynamics).

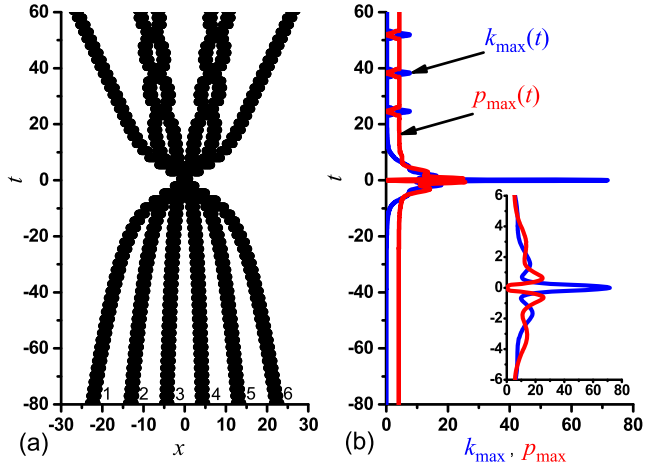

FIG. 9 (color online). Same as in Fig. 8 but for the six-soliton collision. Initial conditions ensure the collision of all six kinks/antikinks at one point (see the text for the details). When the kinetic energy density reaches the maximal value of about 72, the potential energy density is almost zero.

G. Case $N = 7$

In the initial configuration, odd solitons in Fig. 10(a) are the kinks and even are the antikinks. They collide at one point provided that their initial coordinates and velocities are chosen as follows: $x_1 = -x_7 = -39.541867403$, $V_1 = -V_7 = 0.1$, $x_2 = -x_6 = -24.29923$, $V_2 = -V_6 = 0.05$, $x_3 = -x_5 = -12$, $V_3 = -V_5 = 0.025$, and $x_4 = 0$, $V_4 = 0$. Looking at Fig. 10(b) we note that at the collision point the maximal over x kinetic energy density is extremely small, while the maximal potential energy density features a maximum of 94.90 for $h = 0.1$ and 99.56 for $h = 0.05$. It can then be stated that

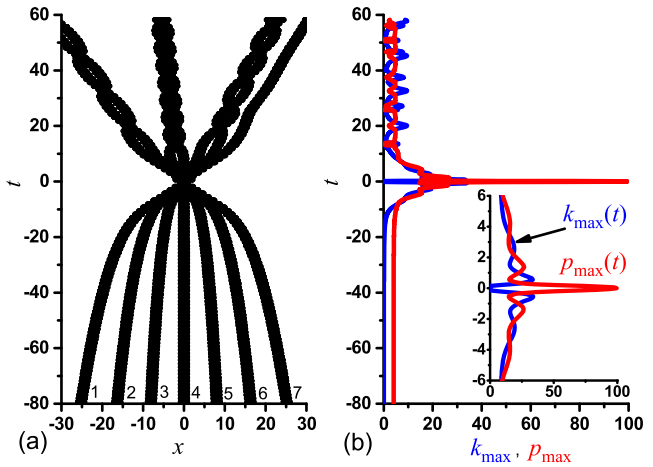

FIG. 10 (color online). Same as in Fig. 8 but for the seven-soliton collision. All seven kinks/antikinks collide at one point due to proper choice of the initial conditions (see the text for the details). When the potential energy density reaches the maximal value of about 100, the kinetic energy density is almost zero.

$$e_{\max}^{(7)} = p_{\max}^{(7)} \approx 100. \quad (26)$$

The case of Fig. 10 is once again one of a pronounced asymmetric outcome, as we have generally observed odd N cases to be (cf. Fig. 8). Three breathers are observed to form (solitons 2–3, 4–5, and 6–7), while the first soliton moves to the right in an isolated trajectory.

IV. EFFECT OF PERTURBATIONS AND SENSITIVITY TO INITIAL CONDITIONS

So far the integrable SGE was analyzed. In many applications various perturbative terms should be taken into account and thus, it is important to see how the results presented in Sec. III are modified by nonintegrable perturbations. There exist two major classes of the perturbations, the Hamiltonian (i.e., energy conserving) and non-Hamiltonian (e.g., dissipative) ones. We have seen that the maximal energy density is in the form of kinetic (potential) energy for the collisions of even (odd) number of kinks and antikinks. Taking into account this qualitative difference, we will consider the effect of perturbations on the three- and four-kink collisions.

The initial conditions are as follows. For the three-kink collisions we simulate a kink with zero velocity $V_2 = 0$ located at the origin ($x_2 = 0$) and the two antikinks with the velocities $V_{1,3} = \pm 0.1$ coming from the initial positions $x_{1,3} = \mp 9$, respectively. For the four-kink collisions we consider a kink-antikink pair with the velocities $V_{2,3} = \pm 0.05$ and initial positions $x_{2,3} = \mp 6$, and another antikink-kink pair with velocities $V_{1,4} = \pm 0.1$ coming from $x_{1,4} = \mp(12 + \delta)$, where a small parameter δ is chosen to achieve maximal energy density at the collision point. Only weak perturbations are analyzed so that the exact kink and kink-antikink solutions to the integrable SGE are employed for setting initial conditions.

A. Effect of discreteness

Here we consider the weak discreteness of the medium as an example of the Hamiltonian perturbation. In fact, numerical integration results presented in Sec. III already reflect the effect of discreteness of spatial and temporal variable. Now we analyze the effect of spatial discreteness more systematically for the three- and four-kink collisions. We integrate Eq. (12) for different values of the lattice spacing $h = \{0.05, 0.1, 0.15, 0.2\}$ and calculate the maximal energy density. We have checked that the effect of temporal discretization with the time step $\tau = 0.005$ can be neglected in comparison to the effect of the spatial discreteness with $h \geq 0.05$.

The obtained results are presented in Fig. 11 for (a) three-kink and (b) four-kink collisions. The numerical points are least squares fitted to the square parabolas: (a) $e_{\max} = 20.07 - 13.7h^2$ and (b) $e_{\max} = 32.13 + 3.37h - 7.54h^2$. At

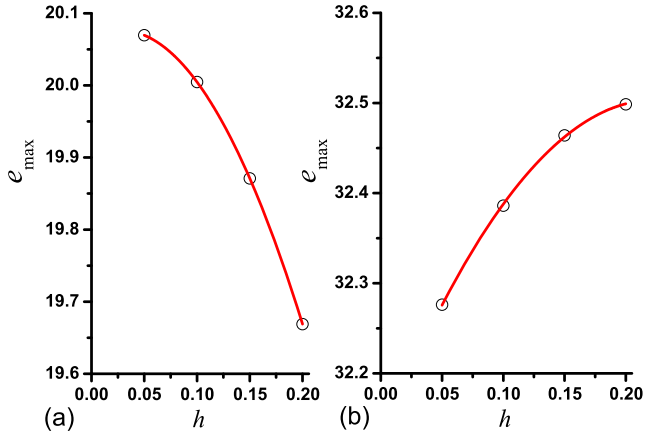

FIG. 11 (color online). Effect of weak discreteness on the maximal energy density in (a) three-kink and (b) four-kink collisions. Results of numerical integration of the discrete model Eq. (12) with the time step $\tau = 0.005$ using the numerical scheme with the accuracy $O(\tau^4)$.

$h = 0$ one has $e_{\max} = 20.07$ in three-kink collision which is very close to the exact result of $e_{\max} = 20$ found in Sec. III C. Similarly, for the four-kink collision from the fitting parabola at $h = 0$ one has $e_{\max} = 32.13$, which is close to the value of 32 estimated in Sec. III D. Interestingly, for the three-kink collision $e_{\max}$ decreases with increasing h and the opposite trend is observed for the four-kink collision. This qualitative difference is not surprising in the light of the fact that in the former case $e_{\max}$ is in the form of potential energy, while in the latter one, it is in the form of kinetic energy.

We conclude that the energy-conserving perturbation of the integrable SGE can lead to either a decrease or increase of the maximal energy density during multisoliton collisions. However, the key finding is that a weak perturbation results in a small change of the maximal energy density.

B. Effect of damping

To study the effect of a non-Hamiltonian perturbation let us introduce the damping term $\gamma(d\phi_n/dt)$ in the left-hand side of the discrete model Eq. (12), where γ is the damping coefficient. This equation is integrated numerically for different values of γ, for the lattice spacing $h = 0.05$ and time step $\tau = 0.005$ using the numerical scheme of accuracy $O(\tau^4)$.

The results are presented in Fig. 12 for (a) three-kink and (b) four-kink collisions. Numerical data are least squares fitted to the linear functions: (a) $e_{\max} = 20.04 - 79.6\gamma$ and (b) $e_{\max} = 32.31 - 532.6\gamma$. At $\gamma = 0$ one has $e_{\max} = 20.04$ in the case of three-kink collision and $e_{\max} = 32.31$ for the four-kink collision. These values are close to those reported in Secs. III C and III D, respectively. In both cases $e_{\max}$ decreases linearly with increasing γ and the slope of the line in the case of the four-kink collision is 1 order of magnitude larger than in the case of the three-kink collision. This result

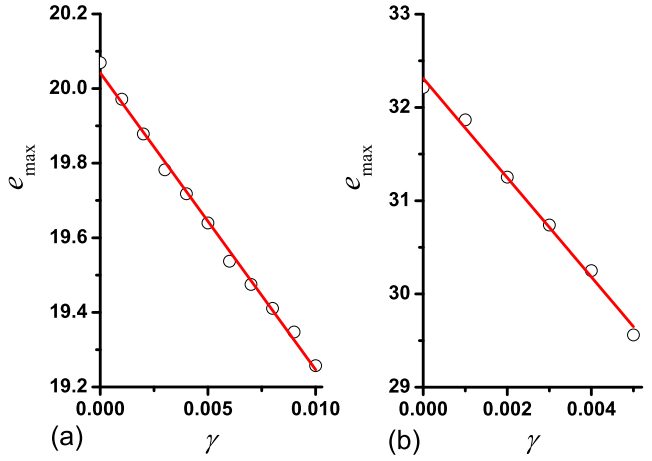

FIG. 12 (color online). Effect of weak damping on the maximal energy density in (a) three-kink and (b) four-kink collisions. Results of numerical integration of the discrete model Eq. (12) with the additional damping term $\gamma(d\phi_n/dt)$ in the left-hand side for the lattice spacing $h = 0.05$ and time step $\tau = 0.005$ using the numerical scheme with the accuracy $O(\tau^4)$.

is expected because, again, unlike the three-kink collision, in the four-kink collision $e_{\max}$ is in the form of kinetic energy when the dashpot damping proportional to the velocity, considered here, is most efficient.

It can be concluded that weak damping reduces the maximal energy in multikink collisions proportionally to the damping coefficient. The effect is much weaker for the collisions of an odd number of kinks when $e_{\max}$ is in the form of potential energy, in comparison to the case when an even number of kinks participates in a collision and $e_{\max}$ is in the form of kinetic energy.

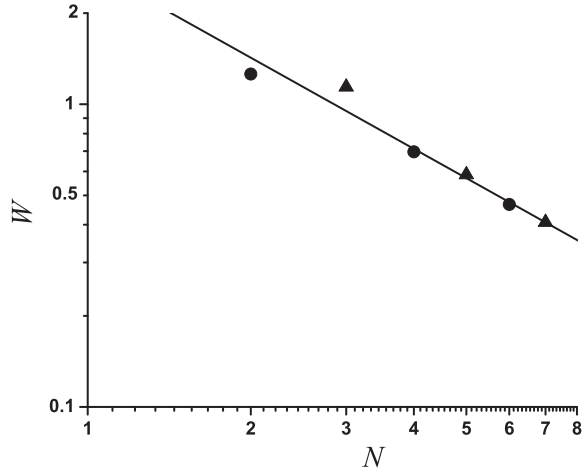

FIG. 13. Full width at half maximum for the high energy density spots as the function of the number of colliding solitons. Different symbols are used for odd and even N. Slope of the line in the log-log plot is equal to -1, so that $W \sim N^{-1}$.

C. Sensitivity to initial conditions

Another issue that is important for applications is the sensitivity of the maximal energy density to the initial conditions (initial positions and velocities of the kinks and antikinks). The full width at half maximum of the high energy density spots can be used as a measure of the accuracy in the initial positions of the kinks required to collide at nearly one point. In Fig. 13 the full width at half maximum of the high energy density spots observed in the collisions of N kinks is presented in the log-log scale as the function of N. The results for even (odd) N are shown by circles (triangles). The slope of the line is -1. We conclude that W reduces with increasing N as $W \sim N^{-1}$. This means that for a larger number of N the sensitivity to the initial conditions increases because the width of the high energy density spots reduces.

V. CONCLUSIONS AND FUTURE CHALLENGES

In this work, we have provided a systematic calculation of the maximal energy density in the collision of N slow kinks/antikinks (with $N \leq 7$) in the integrable sine-Gordon model. Our findings are collected in Table I. The first line gives the number of colliding solitons, N. The second line gives the *exact* values of the maximal energy density that can be achieved in the collision of N kinks/antikinks. These results are available for $N \leq 3$ (see Secs. III A, III B, and III C). For larger N the results were obtained numerically and they are presented in the third and fourth lines of Table I for $h = 0.1$ and $h = 0.05$, respectively. In numerical simulations the kink/antikink velocities are small (no greater than 0.1) but not equal to zero at $t \to \pm\infty$. For decreasing h and decreasing initial velocities of the colliding kinks/antikinks the numerical results converge to the integer numbers shown in the last two lines of Table I.

The results can be summarized as follows. The maximal energy density that can be achieved in collision of N slow kinks/antikinks in SGE is found to be equal to

$$e_{\max}^{(N)} \approx 2N^2 \quad \text{for even } N,$$
$$e_{\max}^{(N)} \approx 2(N^2+1) \quad \text{for odd } N. \tag{27}$$

When an even number of slow kinks/antikinks collides at one point, the kinetic energy density reaches a maximal

TABLE I. Summary on maximal energy density in collision of N solitons for $N \leq 7$.

N	0	1	2	3	4	5	6	7
Exact	0	4	8	20	⋯	⋯	⋯	⋯
$h = 0.1$					32.21	50.93	72.62	94.90
$h = 0.05$					32.05	51.85	72.08	99.56
$2N^2$	0	⋯	8	⋯	32	⋯	72	⋯
$2(N^2+1)$	⋯	4	⋯	20	⋯	52	⋯	100

value $2N^2$, while the maximal potential energy density is nearly equal to zero. On the contrary, when an odd number of slow kinks/antikinks collides at one point, the potential energy density has maximal value $2(N^2+1)$, while the maximal kinetic energy density is almost zero.

These maximal energy density values can be achieved when all N kinks/antikinks collide at one point. This happens when the kinks and antikinks approach the collision point alternatively (i.e., no two adjacent solitons are of the same type). Arranged in this way, each soliton has nearest neighbors of the opposite topological charge. Such solitons attract each other and their cores can merge producing a controllably high energy density spot, as we have demonstrated herein.

As demonstrated in Sec. IV, weak Hamiltonian perturbations can increase or decrease the maximal energy density in soliton collisions. Damping decreases the maximal energy density. The effect of damping is relatively weak for the collisions of an odd number of kinks when the maximal energy density is in the form of the potential energy and is much more pronounced for the collisions of an even number of kinks accompanied by kinetic energy bursts.

According to Eq. (27), the maximal energy density in the sine-Gordon field that can be realized in N-soliton collisions increases quadratically with N. At the same time, total energy of N standing kinks is equal to $8N$ and thus, is proportional to N. Naturally, this does not lead to a contradiction since the very high energy density is accumulated at a very narrow region near $x=0$, and hence when integrated over space, still preserves the total energy of $8N$. The results presented in Fig. 13 support this conclusion. Indeed, the amplitude of the high energy density spot increases as N^2 but its width reduces as N^{-1}, so that its total energy is proportional to N. Furthermore, this very high concentration of energy density for a very short time interval (around $t=0$) is reminiscent of rogue events in other models (such as the nonlinear Schrödinger equation and variants thereof, with their Peregrine soliton and related solutions) [24,25]. However, to the best of our knowledge, no explicit rogue waveforms have been identified yet in such models. Hence, our identification of controllably large energy densities in the SGE model is, arguably, the first example of such a rogue event in this setting.

Having the results of this work in mind, one can expect that in the soliton gas model [33,34] unlimited energy density can be achieved. Of course, the probability of collision of N alternating kinks and antikinks decreases rapidly with increasing N (and even then, the probability of their concurrent collision is very low), but such rare events can have important consequences, when they do arise.

As for the open problems, it is important to calculate the maximal energy density that can be achieved in multisoliton collisions in other integrable and nonintegrable systems of different dimensionality. For example, one can examine similar issues and design such collisions in other Klein-Gordon field theoretic models (e.g. in the ϕ^4 or ϕ^6 models [15,35]), as well as in the one-dimensional, self-defocusing nonlinear Schrödinger equation. It would be particularly interesting to explore if the relevant phenomenology persists therein. It would also be particularly interesting to explore to attempt to prove the asymptotic statements inferred herein; although perhaps a direct approach towards this starting from a multisoliton solution could be very cumbersome, perhaps a reverse approach, initializing the system with a suitably large, and highly localized, energy density at a point and utilizing the inverse scattering transform to establish that this waveform will split into N soliton solutions may be more tractable.

ACKNOWLEDGMENTS

D. S. thanks the financial support of the Institute for Metals Superplasticity Problems, Ufa, Russia. S. V. D. thanks financial support provided by the Russian Science Foundation Grant No. 14-13-00982. The work was supported by the Russian Federation Government Program 5-100-2020. P. G. K. acknowledges support from the U.S. National Science Foundation under Grant No. DMS-1312856, from FP7-People under Grant No. IRSES-605096 from the Binational (U.S.-Israel) Science Foundation through Grant No. 2010239, and from the U.S.-AFOSR under Grant No. FA9550-12-10332.

[1] A. C. Scott, Am. J. Phys. **37**, 52 (1969).
[2] *The Sine-Gordon Model and Its Applications: From Pendula and Josephson Junctions to Gravity and High Energy Physics*, edited by J. Cuevas-Maraver, P. G. Kevrekidis, and F. Williams (Springer, Berlin, 2014).
[3] L. P. Eisenhart, *A Treatise on the Differential Geometry of Curves and Surfaces* (Ginn and Co., Boston, 1909).
[4] S. Watanabe, H. S. J. van der Zant, S. H. Strogatz, and T. P. Orlando, Physica (Amsterdam) **97D**, 429 (1996).
[5] J. K. Perring and T. H. R. Skyrme, Nucl. Phys. **31**, 550 (1962).
[6] S. Coleman, Phys. Rev. D **11**, 2088 (1975).
[7] O. M. Braun and Y. S. Kivshar, *The Frenkel-Kontorova Model: Concepts, Methods, and Applications* (Springer, Berlin, 2004).

[8] E. G. Ekomasov, R. R. Murtazin, O. B. Bogomazova, and A. M. Gumerov, J. Magn. Magn. Mater. **339**, 133 (2013).
[9] S. V. Dmitriev, K. Abe, and T. Shigenari, Physica (Amsterdam) **147D**, 122 (2000).
[10] S. V. Dmitriev, K. Abe, and T. Shigenari, J. Phys. Soc. Jpn. **65**, 3938 (1996).
[11] P. G. Drazin, in *London Mathematical Society Lecture Note Series*, Vol. 85 (Cambridge University Press, Cambridge, 1983).
[12] A. Barone, F. Esposito, C. J. Magee, and A. C. Scott, Riv. Nuovo Cimento **1**, 227 (1971).
[13] Y. S. Kivshar and B. A. Malomed, Rev. Mod. Phys. **61**, 763 (1989).
[14] B. Birnir, H. P. McKean, and A. Weinstein, Commun. Pure Appl. Math. **47**, 1043 (1994).
[15] R. K. Dodd, J. C. Eilbeck, J. D. Gibbon, and H. C. Morries, *Solitons and Nonlinear Wave Equations* (Academic Press, London, 1982).
[16] A. P. Fordy, in *Harmonic Maps and Integrable Systems*, edited by A. P. Fordy and J. C. Wood (Vieweg, Wiesbaden, 1994), pp. 7–28.
[17] R. Hirota, J. Phys. Soc. Jpn. **33**, 1459 (1972).
[18] L. A. Ferreira, B. Piette, and W. J. Zakrzewski, Phys. Rev. E **77**, 036613 (2008).
[19] L. Benfatto, C. Castellani, and T. Giamarchi, Phys. Rev. Lett. **99**, 207002 (2007).
[20] Z. Bajnok, L. Palla, and G. Takacs, Nucl. Phys. **B644**, 509 (2002); Z. Bajnok, C. Dunning, L. Palla, G. Takacs, and F. Wagner, Nucl. Phys. **B679**, 521 (2004).
[21] D. M. Hofman and J. M. Maldacena, J. Phys. A **39**, 13095 (2006).
[22] P. Salmi and M. Hindmarsh, Phys. Rev. D **85**, 085033 (2012).
[23] S. B. Gudnason and M. Nitta, Phys. Rev. D **90**, 085007 (2014).
[24] A. Slunyaev, I. Didenkulova, and E. Pelinovsky, Contemp. Phys. **52**, 571 (2011); see also C. Kharif, E. Pelinovsky, and A. Slunyaev, *Rogue Waves in the Ocean* (Springer-Verlag, Berlin, 2009).
[25] Z. Yan, J. Phys. Conf. Ser. **400**, 012084 (2012).
[26] O. Legrand and G. Reinisch, Phys. Lett. A **35**, 3522 (1987).
[27] O. Legrand, Phys. Lett. A **36**, 5068 (1987).
[28] J. G. Caputo and N. Flytzanis, Phys. Rev. A **44**, 6219 (1991).
[29] D. Saadatmand, S. V. Dmitriev, D. I. Borisov, and P. G. Kevrekidis, Phys. Rev. E **90**, 052902 (2014).
[30] S. V. Dmitriev, P. G. Kevrekidis, and Y. S. Kivshar, Phys. Rev. E **78**, 046604 (2008).
[31] A. E. Miroshnichenko, S. V. Dmitriev, A. A. Vasiliev, and T. Shigenari, Nonlinearity **13**, 837 (2000).
[32] S. V. Dmitriev, Y. S. Kivshar, and T. Shigenari, Phys. Rev. E **64**, 056613 (2001).
[33] I. V. Baryakhtar, V. G. Baryakhtar, and E. N. Economou, Phys. Rev. E **60**, 6645 (1999).
[34] I. V. Baryakhtar, V. G. Baryakhtar, and E. N. Economou, Phys. Lett. A **207**, 67 (1995).
[35] V. A. Gani, A. E. Kudryavtsev, and M. A. Lizunova, Phys. Rev. D **89**, 125009 (2014).